J. Phys. B: At. Mol. Opt. Phys. **33** (2000) 2511–2523. Printed in the UK PII: S0953-4075(00)06951-0

Quantum defect theory with deeply closed channels

T W Gorczyca† and N R Badnell‡

† Department of Physics, Western Michigan University, Kalamazoo, MI 49008-5151, USA
‡ Department of Physics and Applied Physics, University of Strathclyde, Glasgow G4 0NG, UK

Received 16 August 1999, in final form 26 January 2000

Abstract. We address the validity and practicality of using multi-channel quantum defect theory (MQDT) to treat electron–ion collision problems for cases where some channel solutions propagate with extremely negative, classically forbidden, energies. We discuss theoretically and demonstrate numerically, within an unrealistically sensitive model-problem study, how MQDT results can be obtained which are in agreement with those obtained from the more standard non-MQDT method at *all* energies.

1. Introduction

Multi-channel quantum defect theory (MQDT) is a powerful method for treating electron–ion collision problems such as those that arise in electron-impact excitation, ionization and recombination studies, and in photoionization studies (see Seaton 1966, 1969, 1983, Greene *et al* 1979, 1982, Aymar *et al* 1996). It is an *analytic* technique for identifying the smooth, usually very weak, energy dependence of pertinent scattering amplitudes below threshold. Because of this, MQDT methods can easily reduce CPU times by orders of magnitude. Also, other powerful techniques, such as the analytic preconvolution of photoabsorption cross sections (Robicheaux 1993), frame transformation methods for including spin–orbit effects in resonances (see, for example, Aymar *et al* 1996), and complex energy methods to include the missing radiative decay of resonances (Robicheaux *et al* 1995), are only practical within an MQDT formalism. The reason for this is that an analytic representation of the closed-channel energy dependence is required. Furthermore, recent developments (Badnell and Seaton 1999) have detailed how higher-order long-range potentials can be included perturbatively within MQDT in a straightforward manner and so MQDT is no longer restricted to pure Coulomb potentials.

Although MQDT is valid mathematically at all energies, care has to be taken in how one treats negative-energy solutions numerically, far away from threshold. At this point, it is helpful to categorize channels according to their energies and various other properties (e.g. orbital angular momentum l). Partitioned-space methods (e.g. R-matrix) separate the configuration space of the scattering or valence electron into an inner region ($r < r_0$), where the inter-electron coupling potential is strong, and an outer region ($r > r_0$), where the coupling potentials are assumed to be negligible or small enough to be treated as a perturbation, and only the Coulomb and centrifugal terms are retained in the (diagonal) potential, $V(r) = -2z/r + l(l+1)/r^2$. For *open* channels (those with energies $\epsilon \geqslant 0$), the outer-region solutions to the equation

$$\left(-\frac{\mathrm{d}^2}{\mathrm{d}r^2} + V(r) - \epsilon\right) f(r) = 0 \tag{1}$$

0953-4075/00/132511+13$30.00

oscillate sinusoidally as $r \to \infty$. Just below threshold ($\epsilon < 0$), where the energy is still greater than the potential for a large region of configuration space, the solutions oscillate in the outer region from the boundary radius, r_0, out to the finite classical turning radius, r_c, at which point $\epsilon = V(r_c)$. The physical solutions in these *weakly closed* channels decay exponentially beyond the classical turning radius.

The classical turning radius eventually becomes less than the boundary radius ($r_c < r_0$) when the channel energy is decreased sufficiently from threshold. These *strongly closed* channels have exponentially decaying solutions in the outer region, and for all practical purposes may not even need to be considered for $r > r_0$ (Greene *et al* 1979). However, they may have appreciable amplitudes in the inner region, provided that the channel energy is greater than the potential, which has a minimum $V_{\min} = -z^2/l(l+1)$ at $r_{\min} = l(l+1)/z$. When the energy is negative enough so that $\epsilon = -z^2/\nu^2 < V_{\min} = -z^2/l(l+1)$ or, equivalently, $\nu < \sqrt{l(l+1)}$, this channel is classically forbidden everywhere for a purely Coulombic potential. At even lower energies, when $\nu < l$, the traditionally defined regular and irregular Coulomb functions can become complex. We refer to these latter channels (with $\nu < l$) as *deeply closed*. While alternative base pairs of real functions can be used instead (Greene 1979, 1980, Ross and Jungen 1994), the physical solutions nevertheless eventually become numerically unstable as $\nu \to 0$. This is due to a creeping linear dependence of the regular and irregular solutions—the exponentially increasing contribution to each swamps the exponentially decreasing one and there is no way to (numerically) recover the linear combination that yields a decaying physical solution. When using MQDT for studying a broad energy region such that some channels span from open, to deeply closed and to the unstable limit $\nu \to 0$, it is necessary to treat these various cases in a unified manner, retaining the smooth analytic behaviour of scattering quantities near threshold while avoiding numerical instability at very low energies.

We have previously implemented an MQDT approach, which treats *all* closed channels as open, within Seaton's unpublished STGF code (Gorczyca and Badnell 1996, 1997, Badnell *et al* 1998). Here we address the issue of deeply closed channels through the study of a model problem that is designed to replicate the worst-case scenario of a deeply closed channel's *observable* effect on a typical electron–ion collision calculation, which we carry out using the Wigner–Eisenbud R-matrix method (Burke and Berrington 1993). A perturbing resonance belonging to a deeply closed channel is forced to coincide in energy with the higher-ν Rydberg region of a weakly closed channel. We assume that a solution has been obtained for the R-matrix inner-region problem (Berrington *et al* 1995). Then, various methods for tackling the solution of the outer-region problem are explored. First, we look at the traditional non-MQDT method, such as is implemented in the outer-region solution to the Wigner–Eisenbud R-matrix approach (Berrington *et al* 1987). Here, exponentially decaying boundary conditions are enforced for all closed channels, so instability is avoided as $\nu \to 0$. Next, we consider a renormalized MQDT approach. Here, we rescale from complex to real regular and irregular Coulomb functions for $\nu < l$—this approach, on the other hand, eventually becomes unstable as $\nu \to 0$. Finally, we consider a hybrid MQDT approach. This is numerically stable at all energies, yet it follows in spirit the traditional MQDT implementation of extracting weakly energy-dependent scattering quantities. In the hybrid MQDT approach, the deeply closed channels have exponentially decaying boundary conditions enforced, leading to an MQDT analytic reduction only within the subspace of the open plus weakly and strongly closed channels. A similar approach has been adopted by many practitioners of the eigenchannel R-matrix method (Aymar *et al* 1996).

The outline of the paper is as follows. The theoretical methodologies are discussed in section 2 (and an appendix) and then the model problem is presented in section 3, including a detailed comparison between the results of the various theoretical methods.

2. Theoretical methodologies

The solution matrix, $\boldsymbol{F}^{\mathrm{in}}(r)$, for the inner region ($r \leqslant r_0$) is usually expressed compactly in terms of the R-matrix (Burke and Berrington 1993, Aymar *et al* 1996)

$$\boldsymbol{R} \equiv \boldsymbol{F}^{\mathrm{in}}(r)\left(\frac{\mathrm{d}}{\mathrm{d}r}\boldsymbol{F}^{\mathrm{in}}(r)\right)^{-1}\Bigg|_{r=r_0}. \tag{2}$$

For an n-channel case, $\boldsymbol{F}^{\mathrm{in}}(r)$ is the (non-unique) $n \times n$ matrix with diagonal r^{l_i+1}-type physical boundary conditions at $r = 0$. A smooth match of the inner- and outer-region solutions and spatial derivatives at $r = r_0$ is obtained via

$$\boldsymbol{R}\left(\frac{\mathrm{d}}{\mathrm{d}r}\boldsymbol{F}^{\mathrm{out}}(r_0)\right) = \boldsymbol{F}^{\mathrm{out}}(r_0). \tag{3}$$

So far, the outer-region boundary conditions have not been specified. We now consider three different approaches to their specification.

2.1. Method 1

Physical boundary conditions are imposed in the customary outer-region solution to the Wigner–Eisenbud R-matrix approach (see, e.g., Berrington *et al* 1987†). These are sinusoidal in the open channels and exponentially decaying in the closed channels, giving rise to the $n \times n_{\mathrm{o}}$ solution matrix

$$\boldsymbol{F}^{\mathrm{out}}(r) = \begin{pmatrix} \boldsymbol{s}_{\mathrm{o}}(r) \\ 0 \end{pmatrix} + \begin{pmatrix} \boldsymbol{c}_{\mathrm{o}}(r) & 0 \\ 0 & \boldsymbol{\theta}_{\mathrm{c}}(r) \end{pmatrix} \begin{pmatrix} \boldsymbol{K}^{\mathrm{phys}}_{\mathrm{oo}} \\ \boldsymbol{K}^{\mathrm{phys}}_{\mathrm{co}} \end{pmatrix} \tag{4}$$

where $\boldsymbol{K}^{\mathrm{phys}}$ is the *physical* reactance matrix, and where the $n_{\mathrm{o}} \times n_{\mathrm{o}}$ diagonal matrices $\boldsymbol{s}_{\mathrm{o}}(r)$ and $\boldsymbol{c}_{\mathrm{o}}(r)$ have, along their respective diagonals, the regular and irregular Coulomb functions for each channel, i, with asymptotic behaviour

$$\begin{aligned} s_i(r) &\underset{r\to\infty}{\sim} \sin\left(k_i r + \frac{z}{k_i}\ln 2k_i r - l_i\pi/2 + \sigma_{l_i}\right) \\ c_i(r) &\underset{r\to\infty}{\sim} \cos\left(k_i r + \frac{z}{k_i}\ln 2k_i r - l_i\pi/2 + \sigma_{l_i}\right) \end{aligned} \tag{5}$$

where k_i is the channel wavenumber, l_i is the orbital angular momentum, z is the asymptotic charge of the target ion and σ_{l_i} is the usual Coulomb phase shift.

The $n_{\mathrm{c}} \times n_{\mathrm{c}}$ diagonal matrix $\boldsymbol{\theta}_c$ has, instead, exponentially decaying functions along its diagonal which are given by (Seaton 1985)

$$\theta_i(r) = r^{\nu_i}\mathrm{e}^{-zr/\nu_i}\sum_n B_{ni}r^{-n}. \tag{6}$$

The coefficients B_{ni} are computed by standard asymptotic recursion relations. Therefore, they are stable for deeply closed channels since r_0 can be treated as asymptotic and only the first term in the expansion is needed.

† As implemented in STGF.

2.2. Method 2

The essence of MQDT (Seaton 1966, 1983) is that the strong energy dependence of $\boldsymbol{K}^{\rm phys}$ near threshold can be circumvented by matching to solutions that are nearly energy independent there. These *unphysical* outer-region solutions, with closed-channel solutions that diverge exponentially as $r \rightarrow \infty$, take the $n \times n$ matrix form

$$\boldsymbol{F}^{\rm out}(r) = \begin{pmatrix} \boldsymbol{s}_{\rm o}(r) & 0 \\ 0 & \boldsymbol{s}_{\rm c}(r) \end{pmatrix} + \begin{pmatrix} \boldsymbol{c}_{\rm o}(r) & 0 \\ 0 & \boldsymbol{c}_{\rm c}(r) \end{pmatrix} \begin{pmatrix} \boldsymbol{K}_{\rm oo} & \boldsymbol{K}_{\rm oc} \\ \boldsymbol{K}_{\rm co} & \boldsymbol{K}_{\rm cc} \end{pmatrix}. \tag{7}$$

The open-channel solutions $\boldsymbol{s}_{\rm o}(r)$ and $\boldsymbol{c}_{\rm o}(r)$ are the same as those found in method 1. However, here, $\boldsymbol{K}$ is the *unphysical* reactance matrix since the $n_{\rm c} \times n_{\rm c}$ diagonal matrices $\boldsymbol{s}_{\rm c}(r)$ and $\boldsymbol{c}_{\rm c}(r)$, which match smoothly from below threshold to their open-channel counterparts above threshold, now have along their respective diagonals the unphysical exponentially diverging solutions

$$s_i(r) = \frac{A^{1/2}}{2^{1/2}} f_i(r) \qquad \text{and} \qquad c_i(r) = -\frac{1}{2^{1/2} A^{1/2}} \left(g_i(r) + \mathcal{G} f_i(r)\right). \tag{8}$$

Here, f_i and g_i are analytic functions in energy and they are evaluated via series expansions (see Seaton 1983). The parameter A has an energy dependence which is given by

$$A(\nu, l) = \prod_{p=0}^{l} \left(1 - p^2/\nu^2\right) \tag{9}$$

and it therefore alternates between positive and negative values, for $\nu < l$. This gives rise to complex s_i and c_i solutions for deeply closed channels, in the latter case. The closed-channel solutions have asymptotic forms, to within a common factor, given by

$$\begin{aligned} s_i(r) &\underset{r\rightarrow\infty}{\sim} -r^{\nu_i} {\rm e}^{-zr/\nu_i} \cos(\pi\nu_i) + B(\nu_i)\, r^{-\nu_i} {\rm e}^{+zr/\nu_i} \sin(\pi\nu_i) \\ c_i(r) &\underset{r\rightarrow\infty}{\sim} r^{\nu_i} {\rm e}^{-zr/\nu_i} \sin(\pi\nu_i) + B(\nu_i)\, r^{-\nu_i} {\rm e}^{+zr/\nu_i} \cos(\pi\nu_i). \end{aligned} \tag{10}$$

The $n \times n$ unphysical solutions of equation (7) are projected onto the $n \times n_{\rm o}$ physical ones (4) by right-multiplying equation (7) with the transformation matrix

$$\boldsymbol{M} = \begin{pmatrix} \boldsymbol{1}_{\rm oo} \\ \boldsymbol{M}_{\rm co} \end{pmatrix}. \tag{11}$$

Only exponentially decaying solutions remain for the closed channels provided that $\boldsymbol{M}_{\rm co}$ is chosen to be

$$\boldsymbol{M}_{\rm co} = -\left[\boldsymbol{K}_{\rm cc} + \tan(\pi\boldsymbol{\nu}_{\rm c})\right]^{-1} \boldsymbol{K}_{\rm co}. \tag{12}$$

This projection transforms the smooth *unphysical* reactance matrix into the *physical* reactance matrix via

$$\begin{aligned} \boldsymbol{K}^{\rm phys} &= \begin{pmatrix} \boldsymbol{K}_{\rm oo} & \boldsymbol{K}_{\rm oc} \\ \boldsymbol{K}_{\rm co} & \boldsymbol{K}_{\rm cc} \end{pmatrix} \begin{pmatrix} \boldsymbol{1}_{\rm oo} \\ \boldsymbol{M}_{\rm co} \end{pmatrix} \\ &= \begin{pmatrix} \boldsymbol{K}_{\rm oo} - \boldsymbol{K}_{\rm oc} \left[\boldsymbol{K}_{\rm cc} + \tan(\pi\boldsymbol{\nu}_{\rm c})\right]^{-1} \boldsymbol{K}_{\rm co} \\ \boldsymbol{K}_{\rm co} - \boldsymbol{K}_{\rm cc} \left[\boldsymbol{K}_{\rm cc} + \tan(\pi\boldsymbol{\nu}_{\rm c})\right]^{-1} \boldsymbol{K}_{\rm co} \end{pmatrix}. \end{aligned} \tag{13}$$

Although this MQDT method is mathematically equivalent to the previous non-MQDT method (method 1), only much more efficient, some practical issues arise on implementing it numerically for the case of deeply closed channels. Firstly, for $\nu < l$, the traditionally defined regular and irregular Coulomb functions can become complex (see equation (9)). However,

a simple rescaling of complex to real functions, with an accompanying minor modification to the above equation (13), recovers the same *physical* reactance matrix as we detail in an appendix to the present paper. We have implemented this approach within STGF. Secondly, as the effective quantum number ν gets very small, the exponentially increasing components of the s and c functions in equation (10) dominate the exponentially decreasing components and so the s and c functions become (numerically) linearly dependent and the *unphysical* reactance matrix, $\boldsymbol{K}$, becomes unstable.

2.3. Method 3

As we illustrate in the next section, the non-MQDT method suffers from a dramatic energy dependence in the near-threshold reactance matrix, whereas the traditional MQDT method, even after rescaling, becomes unstable for very deeply closed channels as $\nu \to 0$. We have implemented a third method within STGF. This relies on a hybrid approach: exponentially decaying boundary conditions using θ_i are imposed for all deeply closed channels, but the s_i and c_i functions are used for all (unphysical) strongly and weakly closed channels, and all open channels of course. (Partitioning has been discussed formally by Seaton (1969, 1983).) This retains the power of analytically revealing the infinite resonance structure of the weakly closed channels within an MQDT description, while avoiding the instability associated with (very) deeply closed channels. Accordingly, we partition the n-total channel problem into n_o open channels, n_c weakly and strongly closed channels and $n_{\bar{\mathrm{c}}}$ deeply closed channels. The $n \times (n_\mathrm{o} + n_\mathrm{c})$ outer-region solution matrix is taken to be

$$\boldsymbol{F}^{\mathrm{out}}(r) = \begin{pmatrix} \boldsymbol{s}_\mathrm{o}(r) & 0 \\ 0 & \boldsymbol{s}_\mathrm{c}(r) \\ 0 & 0 \end{pmatrix} + \begin{pmatrix} \boldsymbol{c}_\mathrm{o}(r) & 0 & 0 \\ 0 & \boldsymbol{c}_\mathrm{c}(r) & 0 \\ 0 & 0 & \boldsymbol{\theta}_{\bar{\mathrm{c}}} \end{pmatrix} \begin{pmatrix} \boldsymbol{K}^{\mathrm{hyb}}_{\mathrm{oo}} & \boldsymbol{K}^{\mathrm{hyb}}_{\mathrm{oc}} \\ \boldsymbol{K}^{\mathrm{hyb}}_{\mathrm{co}} & \boldsymbol{K}^{\mathrm{hyb}}_{\mathrm{cc}} \\ \boldsymbol{K}^{\mathrm{hyb}}_{\bar{\mathrm{c}}\mathrm{o}} & \boldsymbol{K}^{\mathrm{hyb}}_{\bar{\mathrm{c}}\mathrm{c}} \end{pmatrix} \tag{14}$$

giving rise to a smooth, stable, *hybrid* reactance matrix, $\boldsymbol{K}^{\mathrm{hyb}}$. We now have to project onto physical solutions, following the procedure prescribed by equations (11)–(13).

3. A model problem study

Calculations have been performed for a simple model problem, which we chose for two reasons. First, it enables us to set up precisely the problem that we wish to study. Second, we have found it difficult to find a real case where deeply closed channels make a significant effect. This is because a deeply closed channel, being classically forbidden, usually corresponds to a channel energy far less than that of the position of its lowest-lying resonances. So, only for uncharacteristically large widths and/or non-Coulombic binding potentials may the effect of a deeply closed channel be non-negligible. In a model, we can set the interaction with the deeply closed channel as large as is necessary so as to produce a sizeable observable effect.

3.1. The model

We consider a variant of the model of Badnell and Seaton (1999). Here, we consider three channels with Rydberg energies $E_1 = 0.0$, $E_2 = 0.5$ and $E_3 (> E_2)$; angular momenta $l_1 = 0$, $l_2 = 1$, $l_3 = 1$ (initially); inner-region boundary at $r_0 = 2$ (initially); outer-region charge $z = 1$. We consider energies E in the range $E_1 < E < E_2$ and refer to channel 1 as open (subscript 'o'), channel 2 as closed (subscript 'c') and channel 3 as deeply closed (subscript '$\bar{\mathrm{c}}$'). The effective quantum number in closed channel i is $\nu_i = 1/[E_i - E]^{-1/2}$.

3.1.1. The inner-region solutions. We assume no inner-region coupling between channels 'c' and '$\overline{\text{c}}$' and take inner-region quantum defects of μ_{o}, μ_{c} and $\mu_{\overline{\text{c}}}$. We take the R-matrix to be given by $R_{\text{oo}} = f_{\text{oo}}/f'_{\text{oo}}$, $R_{\text{cc}} = f_{\text{cc}}/f'_{\text{cc}}$, $R_{\overline{\text{cc}}} = f_{\overline{\text{cc}}}/f'_{\overline{\text{cc}}}$, $R_{\text{oc}} = C_{\text{oc}}$, $R_{\text{co}} = R_{\text{oc}}$, $R_{\text{o}\overline{\text{c}}} = C_{\text{o}\overline{\text{c}}}$, $R_{\overline{\text{c}}\text{o}} = R_{\text{o}\overline{\text{c}}}$, $R_{\text{c}\overline{\text{c}}} = 0$ and $R_{\overline{\text{c}}\text{c}} = 0$. Here, $f_{\text{oo}} = (s_{\text{o}}\cos(\pi\mu_{\text{o}}) + c_{\text{o}}\sin(\pi\mu_{\text{o}}))$, $f_{\text{cc}} = (s_{\text{c}}\cos(\pi\mu_{\text{c}}) + c_{\text{c}}\sin(\pi\mu_{\text{c}}))$ and $f_{\overline{\text{cc}}} = (s_{\overline{\text{c}}}\cos(\pi\mu_{\overline{\text{c}}}) + c_{\overline{\text{c}}}\sin(\pi\mu_{\overline{\text{c}}}))$, evaluated at $r = r_0$.

3.1.2. The outer region. We assume only the pure Coulomb potential.

3.1.3. The three methods. Having set up an inner-region problem, we solve the outer-region problem in three ways, as described in section 2. Method 1 solves it without recourse to MQDT, method 2 uses MQDT—including the approach developed for handling deeply closed channels, while method 3 uses the hybrid-MQDT approach.

3.2. Results from the model

In order to obtain a clearer picture of computed scattering quantities in each of the three methods, we first investigate the behaviour of the computed reactance matrix. We focus on the energy region ($0 < E < 1$) containing the second (weakly closed) channel's Rydberg series, which terminates at $E_2 = 0.5$, and force the third channel to be deeply closed ($\nu_3 < l_3 = 1$) across and below the second threshold by setting $E_3 = 1.6$. Each method yields a different reactance matrix. Method 1 computes the 1×1 *physical* reactance matrix, method 2 the 3×3 *unphysical* reactance matrix and method 3 the 2×2 *hybrid* reactance matrix. The energy dependence of these matrices is seen most easily by considering the *eigenquantum defects*, μ_α, which are the arctangents of the eigenvalues of the operational reactance matrix, divided by π:

$$\boldsymbol{K} = \boldsymbol{U}^{\dagger}\tan(\pi\boldsymbol{\mu})\boldsymbol{U}. \tag{15}$$

The results from each method are shown in figure 1. In method 1, μ_1 turns out to be simply the phase shift δ divided by π ($\mu_1 = \delta/\pi$) and it has an infinite number of oscillations near the second threshold $E \lesssim E_2$. Therefore, it is an impossible quantity to resolve fully at the Rydberg limit and, furthermore, it is not a desirable quantity to work with analytically in this energy region.

In method 2, on the other hand, the eigenquantum defects show a weaker energy dependence near the second threshold. The one associated predominantly with the second channel, μ_2, is flat and nearly zero throughout, due to our choice of $\mu_{\text{o}} = 0$, $\mu_{\text{c}} = 0$, $C_{\text{oc}} = 0.5$, and all other weakly closed interactions turned-off. The others, μ_1 associated with the open channel, and μ_3 associated with the channel 3, are strongly interacting due to our choice of $C_{\text{o}\overline{\text{c}}} = 1.5$; μ_1 behaves quite differently from that resulting from method 1. Note also the discontinuity in the derivatives at $E = 0.6$, corresponding to $\epsilon_3 = E - E_3 = -1$, i.e. $\nu_3 = l_3 = 1$. From equations (7)–(9), we see that as $\nu_3 \to l_3$, $s_3 \to 0$ and $c_3 \to \infty$, so that $K_{3i} \to 0$ and μ_3 goes to zero. For $\nu_3 < l_3$, however, we transform the *unphysical* reactance matrix, as detailed in the appendix to this paper, and so the eigenvalues are transformed likewise.

The smoothest behaviour for the eigenquantum defect is obtained from method 3. The eigenquantum defect that we identify as being predominantly associated with the first channel, μ_1, is almost identical to the background (scaled) phase shift obtained with method 1. The other one, μ_2, resembles predominantly the second channel's quantum defect, obtained with method 2. These eigenquantum defects, being the smoothest in energy, are the most amenable to interpolation (see also Kim and Greene (1988), especially their figure 3, where similar conclusions are drawn).

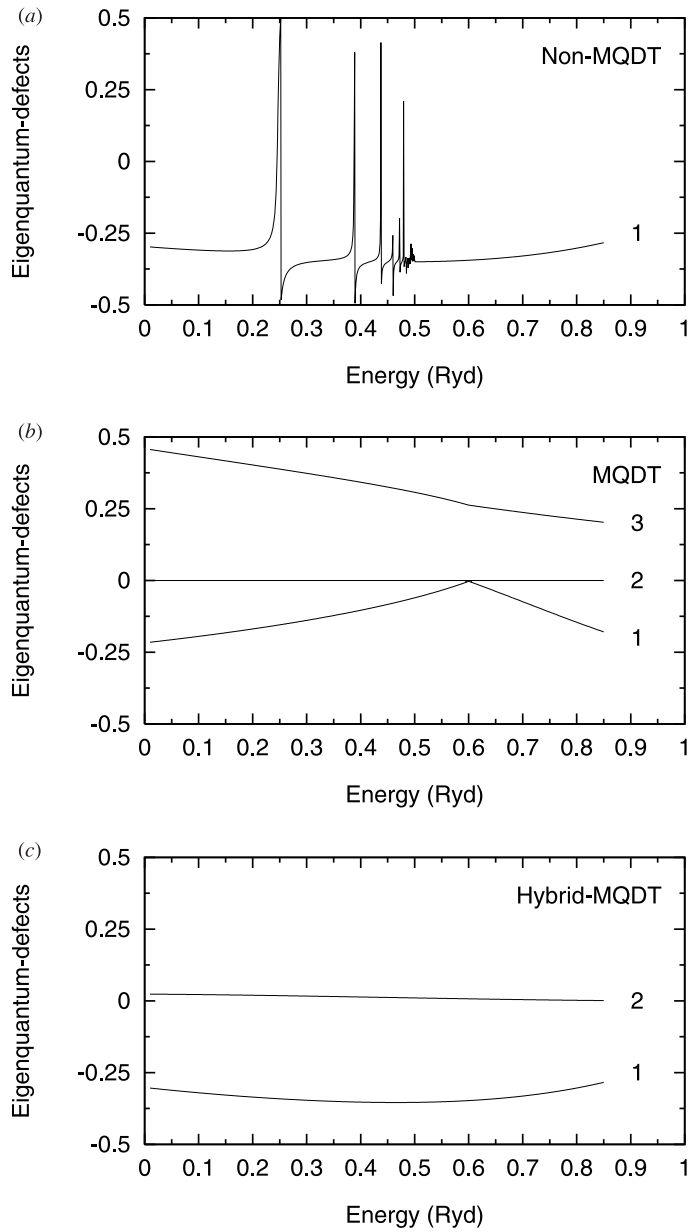

Figure 1. Eigenquantum defects (arctangents of the eigenvalues of the operational reactance matrix divided by π) for: (*a*) method 1, the non-MQDT case, where the 1×1 *physical* reactance matrix $\boldsymbol{K}^{\rm phys}$ is used; (*b*) method 2, the full MQDT case, where the 3×3 *unphysical* reactance matrix $\boldsymbol{K}$ is used (the discontinuity in the derivative at $E = 0.6$ is due to rescaling of $\boldsymbol{K}'$ for $\nu_3 < l_3 = 1$, as discussed in the appendix); and (*c*) method 3, the hybrid MQDT case, where the 2×2 *hybrid* reactance matrix $\boldsymbol{K}^{\rm hyb}$ is used.

Therefore, it is seen that one or the other of the MQDT methods (2 or 3) should be used in order to extract smooth scattering quantities. We now consider the numerical accuracy of

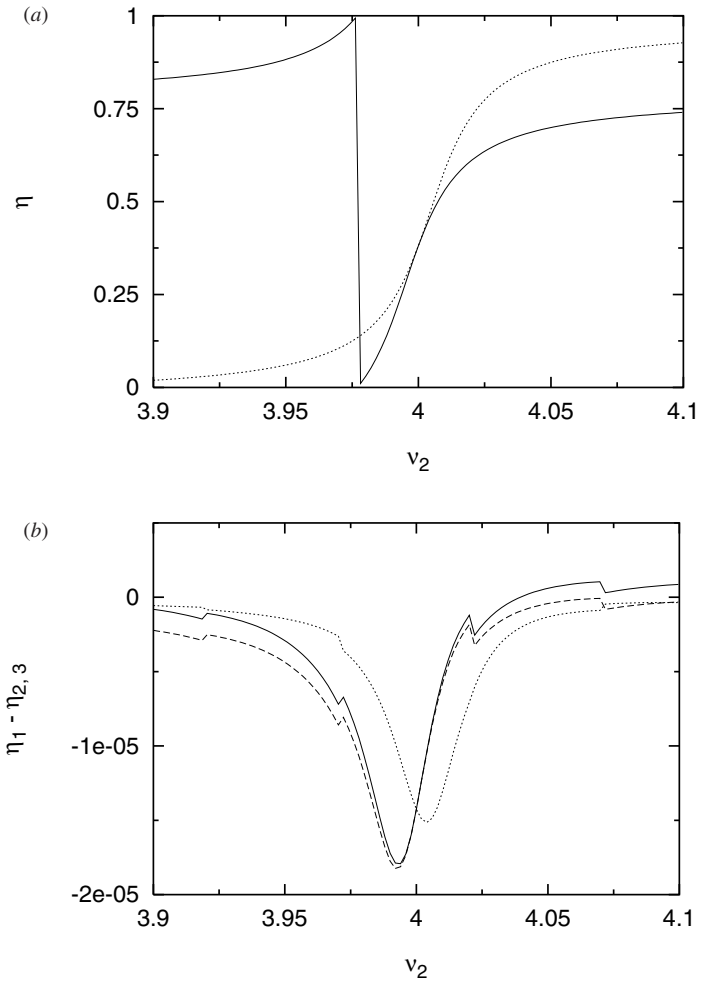

Figure 2. Values of η (the elastic-scattering phase shift is $\pi\eta$) for $E_3 = 1$. Full and broken curves, $C_{o\bar{c}} = 1.5$; dotted curve, $C_{o\bar{c}} = 0$—see text for details. The upper plot shows values of η, and the lower plot the difference between the results from method 1 and methods 2 (broken and dotted curves) and 3 (full and dotted curves).

each method by focusing on the third channel's effect on a single resonance as $\nu_3 \to 0$, obtained by adjusting E_3. We put $\boldsymbol{K}_{oo}^{phys} = \tan(\pi\eta)$: then $\pi\eta$ is the elastic-scattering phase shift. With $\mu_o = 0$, one obtains resonances in the vicinity of $\nu_2 = (n - \mu_c)$, with $\eta \approx \frac{1}{2}$ at $\nu_2 \approx (n - \mu_c)$. The precise form of the resonances depends on the values assigned to C_{oc} and $C_{o\bar{c}}$. On setting $C_{o\bar{c}} = 0$, initially, we find that a value of $C_{oc} = 0.5$ closely reproduces the resonance shown in figure 1 of Badnell and Seaton (1999) and we choose this as the basis for our study. We focus on values for E_3 such that $\nu_3 < l_3 + 0.5$ and so there are no resonances associated with this channel over the range of E studied. This was verified by setting $C_{oc} = 0$, with $C_{o\bar{c}}$ non-zero, and observing a constant value for η. We find that setting $C_{o\bar{c}} = 1.5$ (with $C_{oc} = 0.5$) produces a strong perturbation of η by channel 3. (We note that $C_{o\bar{c}} = 1.5$ is an unphysically large value.)

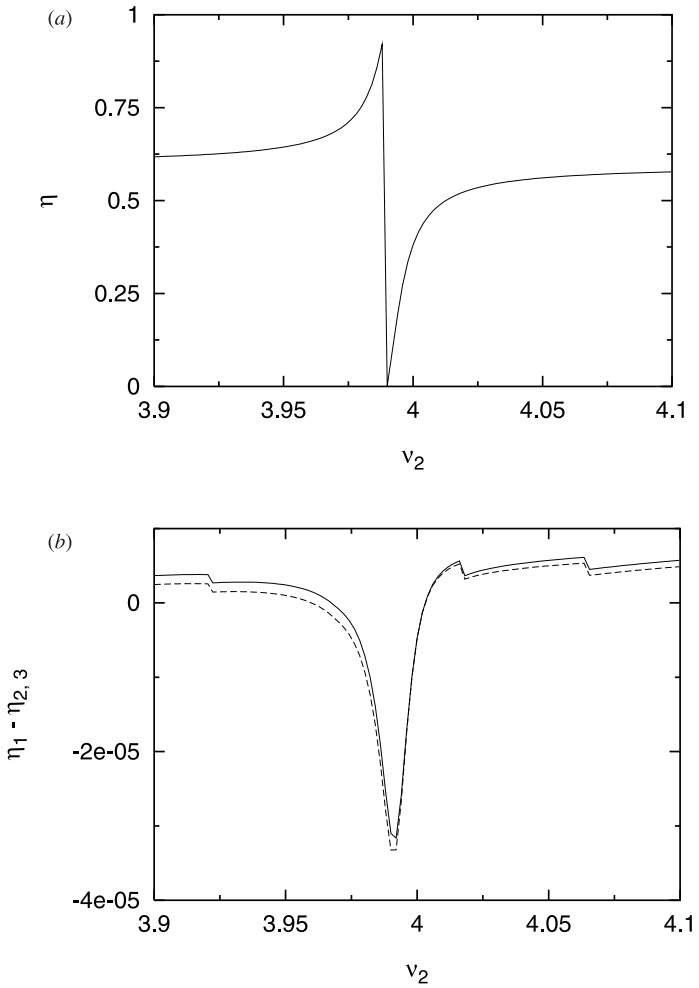

Figure 3. As in figure 2, for $E_3 = 2.2$ ($C_{o\bar{c}} = 1.5$ only).

Figure 2(a) shows η for the $\nu_2 = 4$ resonance, with $\mu_c = 0$. We show results both for $C_{o\bar{c}} = 0$ and 1.5, with $\mu_{\bar{c}} = 0$. We chose $E_3 = 1$, giving values for $\nu_3 \approx 1.3 > l_3$, over the energy range shown. Figure 2(a) shows clearly the effect of channel 3. On this scale, the results from all three methods are indistinguishable. Figure 2(b) shows, on a more expanded scale, values of $\delta\eta = \eta_1 - \eta_{2,3}$. In the vicinity of $\nu_2 = 4$ we have $\eta \approx 0.5$ and $\tan(\pi\eta)$ is large: largish values of $\delta\eta$ then give fractional errors in $\tan(\pi\eta)$ which are quite small. We see that the results of methods 2 and 3 differ little from those of method 1.

Next, we consider $E_3 = 2.2$. This results in values for $\nu_3 \approx 0.75 < l_3$. We keep $C_{o\bar{c}}$ constant as we vary E_3. In reality, of course, $C_{o\bar{c}}$ should decrease as E_3 is moved further away from E_1 and E_2, but a constant value is all that is necessary for our model problem. Figure 3(a) again shows η for the $\nu_2 = 4$ resonance. The results from all three methods are (again) indistinguishable. In figure 3(b), we see that the differences between the results of the methods 2 and 3, compared with method 1, have changed little even though we now have $\nu_3 < l_3$.

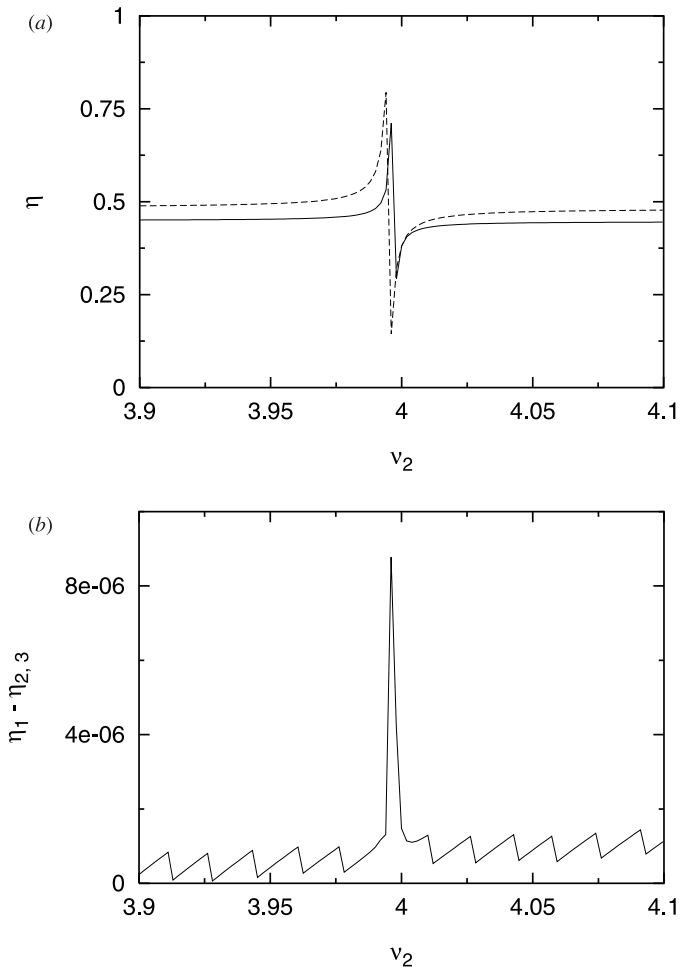

Figure 4. As in figure 2, for $E_3 = 15$ ($C_{o\bar{c}} = 1.5$ only).

Finally, we consider $E_3 = 15.0$. This results in values for $\nu_3 \approx 0.26 \ll l_3$. In figure 4($a$), we now see clear differences between the results, for η, from method 2 and methods 1 and 3, which are indistinguishable. (Note, although these results indicate errors in s_3 and c_3, and we use s and c to define the R-matrix, the same identical R-matrix is used for all three methods and the differences observed in figure 4(a) are due solely to the different treatments of the outer-region problem.) In figure 4(b), we see that the results of the hybrid-MQDT method (method 3) are still subject to only very small errors. (The values of $\eta_1 - \eta_2$ are largely off the scale and so are not shown.)

3.3. Discussion

We have seen that the pure MQDT approach to deeply closed channels (method 2) does break down eventually due to an increasing linear dependence of s and c. We find the onset to be quite rapid and it occurs at $\nu_3 \approx 0.3$ ($l_3 = 1$) for the model considered here. On increasing l_3, we find that this onset occurs at slightly smaller values of ν_3. It is also relatively insensitive

to the value of $C_{o\bar{c}}$, provided that it is not vanishingly small. We also find that it varies with the R-matrix radius—on studying a range of values ($r_0 = 2$–16)—via $\nu_3 \approx r_0/10$. This means that K-shell holes in multi-electron atoms provide the worst-case scenario. However, we emphasize again that we have had to resort to a model problem to observe strong effects from deeply closed channels. In normal situations, we have found in the past that a safe, simple and accurate MQDT approach is to omit channels with $\nu < l$ from both the inner- and outer-region solutions. We have demonstrated that the accuracy of such an approach can be checked purely within MQDT by using our approach for deeply closed channels (method 2) or the hybrid-MQDT method for the most deeply closed channels. Of course, the accuracy can also be checked (and has been routinely) by comparison with the results of a non-MQDT calculation.

4. Conclusion

MQDT methods for treating electron–ion collision problems are mathematically equivalent to non-MQDT ones at *all* scattering energies and, numerically, give the same results (to within the accuracy of the numerical methods used) provided that certain modifications are made, and which we have made in STGF. First, for deeply closed channels, a rescaling of any complex Coulomb functions, and a corresponding modification to the MQDT equations, is necessary—this we detail in the appendix. Second, for extremely low channel energies ($\nu_3 \lesssim r_0/10$ in our model), even a rescaled MQDT method becomes numerically unstable. We circumvent this instability by forcing deeply closed channel solutions to be exponentially decaying prior to the determination of an *unphysical* reactance matrix, as is done for all closed channels in the non-MQDT case. This hybrid-MQDT method is quite useful since, accuracy-wise, numerical instabilities are avoided and the results are the same as non-MQDT ones at *all* energies. Just as importantly, efficiency-wise, an essentially analytic formula is extracted for the infinitely oscillating behaviour of resonant scattering quantities associated with each weakly closed channel; analytic expressions can be used to reduce the computational effort by orders of magnitude and make other analytic techniques applicable. We also note that for realistic situations, rather than our model problem, we have found completely omitting channels with $\nu < l$ to be an accurate and reliable approach.

Acknowledgments

We thank C H Greene and F Robicheaux for several helpful discussions and for comments on an earlier version of this manuscript.

Appendix

We show here how to determine the *physical* reactance matrix when the deeply closed channel solutions are rescaled from complex to real. For $\nu < l$, the parameter A of equation (9) can become negative and so the s_i and c_i functions in equation (8) become complex. If we instead replace A with $-A$, and refer to these new solutions as s_i' and c_i', then our outer-region (unphysical) solution matrix, which we now partition into open (subscript 'o'), weakly and

strongly closed (subscript 'c') and deeply closed (subscript '$\bar{\mathrm{c}}$') blocks, becomes

$$\boldsymbol{F}^{\mathrm{out},\prime}(r) = \begin{pmatrix} \boldsymbol{s}'_{\mathrm{o}}(r) & 0 & 0 \\ 0 & \boldsymbol{s}'_{\mathrm{c}}(r) & 0 \\ 0 & 0 & \boldsymbol{s}'_{\bar{\mathrm{c}}}(r) \end{pmatrix} + \begin{pmatrix} \boldsymbol{c}'_{\mathrm{o}}(r) & 0 & 0 \\ 0 & \boldsymbol{c}'_{\mathrm{c}}(r) & 0 \\ 0 & 0 & \boldsymbol{c}'_{\bar{\mathrm{c}}}(r) \end{pmatrix} \begin{pmatrix} \boldsymbol{K}'_{\mathrm{oo}} & \boldsymbol{K}'_{\mathrm{oc}} & \boldsymbol{K}'_{\mathrm{o}\bar{\mathrm{c}}} \\ \boldsymbol{K}'_{\mathrm{co}} & \boldsymbol{K}'_{\mathrm{cc}} & \boldsymbol{K}'_{\mathrm{c}\bar{\mathrm{c}}} \\ \boldsymbol{K}'_{\bar{\mathrm{c}}\mathrm{o}} & \boldsymbol{K}'_{\bar{\mathrm{c}}\mathrm{c}} & \boldsymbol{K}'_{\bar{\mathrm{c}}\bar{\mathrm{c}}} \end{pmatrix} \tag{A1}$$

where

$$\begin{aligned} \boldsymbol{s}'_{\mathrm{o}}(r) &= \boldsymbol{s}_{\mathrm{o}}(r) \qquad & \boldsymbol{s}'_{\mathrm{c}}(r) &= \boldsymbol{s}_{\mathrm{c}}(r) \qquad & \boldsymbol{s}'_{\bar{\mathrm{c}}}(r) &= \boldsymbol{s}_{\bar{\mathrm{c}}}(r)\,\mathbf{i}^{-1} \\ \boldsymbol{c}'_{\mathrm{o}}(r) &= \boldsymbol{c}_{\mathrm{o}}(r) \qquad & \boldsymbol{c}'_{\mathrm{c}}(r) &= \boldsymbol{c}_{\mathrm{c}}(r) \qquad & \boldsymbol{c}'_{\mathrm{c}}(r) &= \boldsymbol{c}_{\bar{\mathrm{c}}}(r)\,\mathbf{i} \end{aligned} \tag{A2}$$

and $\mathbf{i}$ is just i times the $n_{\bar{\mathrm{c}}} \times n_{\bar{\mathrm{c}}}$ identity matrix. (Alternatively, complex functions can be avoided by reformulating MQDT using different base pairs, such as the f_i and g_i of equation (8); see Greene (1979, 1980), Ross and Jungen (1994).) The projection matrix is now defined as

$$\boldsymbol{M} = \begin{pmatrix} \mathbf{1}_{\mathrm{oo}} \\ \boldsymbol{M}_{\mathrm{co}} \\ \boldsymbol{M}_{\bar{\mathrm{c}}\mathrm{o}} \end{pmatrix}. \tag{A3}$$

Elimination of the divergent behaviour of the weakly, strongly and deeply closed channels is achieved if

$$\begin{pmatrix} \boldsymbol{M}_{\mathrm{co}} \\ \boldsymbol{M}_{\bar{\mathrm{c}}\mathrm{o}} \end{pmatrix} = -\begin{pmatrix} \boldsymbol{K}'_{\mathrm{cc}} + \tan(\pi\boldsymbol{\nu}_{\mathrm{c}}) & \boldsymbol{K}'_{\mathrm{c}\bar{\mathrm{c}}} \\ \boldsymbol{K}'_{\bar{\mathrm{c}}\mathrm{c}} & \boldsymbol{K}'_{\bar{\mathrm{c}}\bar{\mathrm{c}}} - \tan(\pi\boldsymbol{\nu}_{\bar{\mathrm{c}}}) \end{pmatrix}^{-1} \begin{pmatrix} \boldsymbol{K}'_{\mathrm{co}} \\ \boldsymbol{K}'_{\bar{\mathrm{c}}\mathrm{o}} \end{pmatrix}. \tag{A4}$$

The *physical* reactance matrix is then given by

$$\boldsymbol{K}^{\mathrm{phys}}_{\mathrm{oo}} = \boldsymbol{K}'_{\mathrm{oo}} - \begin{pmatrix} \boldsymbol{K}'_{\mathrm{oc}} & \boldsymbol{K}'_{\mathrm{o}\bar{\mathrm{c}}} \end{pmatrix} \begin{pmatrix} \boldsymbol{K}'_{\mathrm{cc}} + \tan(\pi\boldsymbol{\nu}_{\mathrm{c}}) & \boldsymbol{K}'_{\mathrm{c}\bar{\mathrm{c}}} \\ \boldsymbol{K}'_{\bar{\mathrm{c}}\mathrm{c}} & \boldsymbol{K}'_{\bar{\mathrm{c}}\bar{\mathrm{c}}} - \tan(\pi\boldsymbol{\nu}_{\bar{\mathrm{c}}}) \end{pmatrix}^{-1} \begin{pmatrix} \boldsymbol{K}'_{\mathrm{co}} \\ \boldsymbol{K}'_{\bar{\mathrm{c}}\mathrm{o}} \end{pmatrix}. \tag{A5}$$

Thus, we can work with rescaled Coulomb functions, giving a *modified unphysical* reactance matrix, $\boldsymbol{K}'$, that can still be used to produce a *physical* reactance matrix, provided that we simply reverse the sign of the $\tan(\pi\nu_i)$ term for every deeply closed channel.

Finally, the *physical* scattering matrix is given by

$$\boldsymbol{S}^{\mathrm{phys}} = (\mathbf{1} + \mathbf{i}\,\boldsymbol{K}^{\mathrm{phys}})(\mathbf{1} - \mathbf{i}\,\boldsymbol{K}^{\mathrm{phys}})^{-1}. \tag{A6}$$

Defining the *unphysical* scattering matrix via

$$\boldsymbol{S} = (\mathbf{1} + \mathbf{i}\,\boldsymbol{K})(\mathbf{1} - \mathbf{i}\,\boldsymbol{K})^{-1} \tag{A7}$$

one obtains

$$\boldsymbol{S}^{\mathrm{phys}}_{\mathrm{oo}} = \boldsymbol{S}_{\mathrm{oo}} - \boldsymbol{S}_{\mathrm{oc}}[\boldsymbol{S}_{\mathrm{cc}} - \exp(-2\pi\mathrm{i}\boldsymbol{\nu}_{\mathrm{c}})]^{-1}\boldsymbol{S}_{\mathrm{co}}. \tag{A8}$$

Deeply closed channels can be taken account of by reversing the sign of ν_i for these channels and generalizing the partitioning of equation (A8) analogously to (A5), together with replacing $\boldsymbol{S}$ by $\boldsymbol{S}'$.

References

Aymar M, Greene C H and Luc-Koenig E 1996 *Rev. Mod. Phys.* **68** 1015–23
Badnell N R, Gorczyca T W and Price A D 1998 *J. Phys. B: At. Mol. Opt. Phys.* **31** L239–48
Badnell N R and Seaton M J 1999 *J. Phys. B: At. Mol. Opt. Phys.* **32** 3955–64
Berrington K A, Burke P G, Butler K, Storey P J, Taylor K T and Yu Yan 1987 *J. Phys. B: At. Mol. Phys.* **20** 6379–97
Berrington K A, Eissner W B and Norrington P H 1995 *Comput. Phys. Commun.* **92** 290–420
Burke P G and Berrington K A 1993 *Atomic and Molecular Processes: an R-matrix Approach* (Bristol: IOP Publishing)
Gorczyca T W and Badnell N R 1996 *J. Phys. B: At. Mol. Opt. Phys.* **29** L283–90
——1997 *Phys. Rev. Lett.* **79** 2783–6
Greene C H 1979 *Phys. Rev.* A **20** 656–69
——1980 *Phys. Rev.* A **22** 149–57
Greene C H, Fano U and Strinati G 1979 *Phys. Rev.* A **19** 1485–509
Greene C H, Rau A R P and Fano U 1982 *Phys. Rev.* A **26** 2441–59
Kim L and Greene C H 1988 *Phys. Rev.* A **38** 2361–70
Robicheaux F 1993 *Phys. Rev.* A **48** 4162–9
Robicheaux F, Gorczyca T W, Pindzola M S and Badnell N R 1995 *Phys. Rev.* A **52** 1319–33
Ross S C and Jungen Ch 1994 *Phys. Rev.* A **49** 4353–63
Seaton M J 1966 *Proc. Phys. Soc.* **88** 801–14
——1969 *J. Phys. B: At. Mol. Phys.* **2** 5–11
——1983 *Rep. Prog. Phys.* **46** 167–257
——1985 *J. Phys. B: At. Mol. Phys.* **18** 2111–31